Chemical Science

ROYAL SOCIETY OF CHEMISTRY

EDGE ARTICLE

View Article Online
View Journal | View Issue

Check for updates

Cite this: *Chem. Sci.*, 2020, **11**, 10737

All publication charges for this article have been paid for by the Royal Society of Chemistry

Open Access Article. Published on 28 mai 2020. Downloaded on 02.06.2026 07.23.18.
This article is licensed under a Creative Commons Attribution 3.0 Unported Licence.

Amination of the Gd@C_{82} endohedral fullerene: tunable substitution effect on quantum coherence behaviors†

Zheng Liu,‡[a] Huan Huang,‡[d] Ye-Xin Wang,[a] Bo-Wei Dong,[a] Bao-Yun Sun, *[d] Shang-Da Jiang *[ab] and Song Gao *[abc]

The core–shell structure of endohedral fullerene-based anisotropic magnetic molecules of high spin with long coherence time could help scale up quantum systems. In this research, by amination of Gd@C_{82} with morpholine, three derivatives are functionalized with 5, 7 and 9 morpholine groups providing an interesting model to investigate the relationship between the quantum coherence and the spin environment. The original radical located on the carbon cage is successfully quenched, affording a quantum phase memory times (T_M) over 5 μs at 5 K. By increasing the number of substitution groups, spin–lattice relaxation times (T_1) also show significant enhancement due to the interaction variation between the molecules and the environments. We found that the T_M of the three molecules show no obvious difference below 10 K, while they are limited by T_1 at higher temperatures. In this work, the variable functional groups are able to tune both T_1 and T_M, offering the possibility for application of high-spin magnetic molecules in the field of quantum information processing.

Received 17th April 2020
Accepted 28th May 2020

DOI: 10.1039/d0sc02182b

rsc.li/chemical-science

Introduction

Endohedral fullerenes with encapsulated metal atoms, ions or clusters in the carbon cage have shown lots of distinctive properties compared to the hollow ones due to the electron transfer between the inner core and the outer shell. Plenty of applications of endohedral fullerenes have been investigated including in chemistry,[1] electronics[2] and reactions.[3] Additionally, paramagnetic endohedral fullerenes containing well protected unpaired electron spins show unique characteristics compared to radicals and complexes. The various paramagnetic properties can be applied in dynamic nuclear polarization (DNP),[4] magnetic resonance imaging (MRI) contrast agents,[5,6] molecular magnets[7] and biomedicines.[8,9]

Recently, quantum information processing (QIP) has been proved to be able to provide efficient solutions in cryptography[10,11] and database searching.[12] Molecular spins, being much more versatile as building blocks, are becoming the competitive one in the area of QIP.[13] The high spin state of molecular magnet-based "qudits" fits the requirements for Grover's algorithm proposed by Leuenberger and Loss.[14] This proposal requires the spin system to possess non-equidistant energy levels and long enough quantum phase memory time. The design of magnetic coordination complexes will give us a chance in fine controlling the quantum coherence and building quantum gates.[15] However, there is a significant contradiction between these conditions since the quantum coherence of an anisotropic high-spin system can be easily destroyed due to its strong coupling to the environment. One possible protocol to solve this problem is to employ rare earth ions of high spin ground state with small anisotropy. The core–shell structures of endohedral fullerenes could fulfill the requirements in QIP,[16,17] and show even better properties compared to other molecule-based qubits. Various paramagnetic endohedral fullerenes show some particular phenomena including the qubit crossover phenomenon[18] and diverse Rabi cycles.[19]

However, most investigations of paramagnetic endohedral fullerenes are limited to pristine molecules. Functionalization of fullerenes can precisely tune the spin environment,[20,21] helping us understand the spin dynamics. Gd@C_{82} is a well-known endohedral fullerene with the paramagnetic metal ion Gd^{3+} of $S = 7/2$ for the inner core and C_{82}^{3-} acting as a radical

[a]*Beijing National Laboratory of Molecular Science, Beijing Key Laboratory of Magnetoelectric Materials and Devices, College of Chemistry and Molecular Engineering, Peking University, Beijing 100871, China. E-mail: jiangsd@pku.edu.cn; gaosong@pku.edu.cn*

[b]*School of Chemistry and Chemical Engineering, South China University of Technology, Guangzhou 510640, China*

[c]*Beijing Academy of Quantum Information Sciences, West Bld. #3, No. 10 Xibeiwang East Rd., Haidian District, Beijing 100193, P. R. China*

[d]*CAS Key Lab for Biomedical Effects of Nanomaterials and Nanosafety, Institute of High Energy Physics, Chinese Academy of Sciences, Beijing 100049, China. E-mail: sunby@ihep.ac.cn*

† Electronic supplementary information (ESI) available. See DOI: 10.1039/d0sc02182b

‡ These authors contributed equally.

Open Access Article. Published on 28 mai 2020. Downloaded on 02.06.2026 07.23.18.
This article is licensed under a Creative Commons Attribution 3.0 Unported Licence.

located at the outer shell. The antiferromagnetic coupling between Gd^{3+} and the radical makes an $S = 3$ ground state.[22] Since the electron cloud of the radical is largely scattered among the outer shell with lack of protection, the properties of the spin system are largely influenced by the environment. This phenomenon is a disadvantage because the uncontrollable interactions will largely reduce the performance of endohedral fullerenes in QIP. The distribution of the electron cloud could enhance the influence of the environment and largely reduce the quantum coherence time. Herein, to overcome this disadvantage, we successfully quench the unwanted shell-radical by amination of the fullerene cage, obtaining three derivatives $Gd@C_{82}(morpholine)_n$ (marked as **Gd-*n***, $n = 5$, 7 and 9).

Results & discussion

In our previous studies,[23,24] the amination of $Gd@C_{82}$ with morpholine and *N*-fluorobenzenesulfonimide (NFSI) resulted in the selective formation of three derivatives, **Gd-5**, **Gd-7** and **Gd-9**. The structure of **Gd-7** has been confirmed by X-ray crystallographic analysis in the previous report. The evidence including UV-Vis-NIR spectroscopy, electrochemical analysis and continuous wave electron paramagnetic resonance (cw-EPR) demonstrated that this series of **Gd-*n*** derivative compounds are functionalized with an odd number of morpholine groups. Different from the original endohedral fullerene $Gd@C_{82}$, the absence of the radical leads to a relatively independent environment with controllable differences. The comparison of this series of molecules provides a very interesting model to investigate the quantum coherence behavior with a tunable environment influence. In this work, we move forward to the different behaviors of the spin–lattice relaxation time (T_1) and quantum phase memory time (T_M).

To evidence the quenching of the radical, the magnetizations of **Gd-7** were measured at 2 K up to 5 T on a magnetometer as shown in Fig. S2-1.† The field-dependent magnetization curve and the saturation value fit best to the $S = 7/2$ model of the Brillouin function. These results confirm the disappearance of the radical in **Gd-*n*** molecules (ESI†).

cw-EPR characterization

In the previous research, the spin system of the $Gd@C_{82}$ endohedral fullerene was considered as the combination of one high spin Gd^{3+} center of $S = 7/2$ and one radical of $S = 1/2$ delocalized on the carbon cage. The two spins were antiferromagnetically coupled as an $S = 3$ system according to high-frequency EPR measurements.[22] However, the radical at the carbon cage reduces the protection of the spin system efficiently, which can be certified from measurements under different conditions. Such influence will also lead to poor quantum coherence properties.

With the shell radical quenched, the Gd^{3+} ion is the only electron spin carrier in the molecules. Even though the first order orbit angular momentum of the Gd^{3+} ion is fully quenched, a slight magnetic anisotropy can still be observed due to the second order spin–orbit coupling in the existence of broken environmental symmetry. $Gd@C_{82}$ and the three derivative compounds were resolved in a d_8-toluene solution with relatively low concentrations from 5 K to 150 K as reported in a previous study. The X-band cw-EPR offers us a way to probe the crystal field effect with various chemical modifications on the fullerene cage. Therefore, the spin Hamiltonian of **Gd-*n*** is considered as

$$\hat{H} = g_{iso}\mu_B B\hat{S} + D\hat{S}_z^{\,2} + E\left(\hat{S}_x^{\,2} - \hat{S}_y^{\,2}\right), \quad (1)$$

where the first term describes the Zeeman effect and the latter two represent the second-rank zero-field splitting (ZFS) of rhombic symmetry. As no significant hyperfine interaction was evidenced in the cw-EPR spectra (^1H, ^2D, ^{14}N, ^{155}Gd or ^{157}Gd), the hyperfine interaction and nuclei quadrupole terms are not included in the Hamiltonian. The simulations of the experimental curves of the derivatives at 20 K (Fig. 1) provided three sets of parameters as the best fitting result for each spectrum, as listed in Table 1. Compared to the Gd^{3+} center of the original $Gd@C_{82}$ molecule, ZFS parameters are different for those of the three derivatives, indicating that the electron spins have rearranged, suggesting differences in quantum coherence behaviors.

Quantum coherence properties

The aforementioned results illustrated that the Gd^{3+} electronic structures can be varied by chemical modification on the outer shell. The protocol for the quantum searching algorithm with molecular magnets proposed by Leuenberger and Loss requires non-equidistant energy levels. The present approach of modifying electronic structures of paramagnetic ions makes the employment of **Gd-*n*** as a qudit ($d = 8$) possible.[25,26] Now we move to study how the substitution groups affect the spin dynamics behaviors. According to the simulations of the cw-EPR spectra of the three derivatives, the D values (0.2–0.3 cm^{-1}) are comparable to the microwave frequency (~9.3 GHz) used in an X-band EPR spectrometer. Only several transitions were observed in the experiments. In the echo-detected field swept (EDFS) experiments, the standard Hahn echo pulse sequence

Table 1 The spin Hamiltonian parameters for the three derivative compounds

Compound	*S*	*g*	*D*	*E*
Gd^{3+} of $Gd@C_{82}$ (ref. 22)	7/2	(2.0090, 2.0100, 1.9775)	0.2575 cm^{-1}	0.0070 cm^{-1}
$Gd@C_{82}(morpholine)_5$ (ref. 24)	7/2	1.96	0.3069 cm^{-1}	0.0280 cm^{-1}
$Gd@C_{82}(morpholine)_7$ (ref. 24)	7/2	1.98	0.2175 cm^{-1}	0.0217 cm^{-1}
$Gd@C_{82}(morpholine)_9$ (ref. 24)	7/2	1.99	0.2542 cm^{-1}	0.0252 cm^{-1}

 This journal is © The Royal Society of Chemistry 2020

Open Access Article. Published on 28 mai 2020. Downloaded on 02.06.2026 07.23.18.
This article is licensed under a Creative Commons Attribution 3.0 Unported Licence.

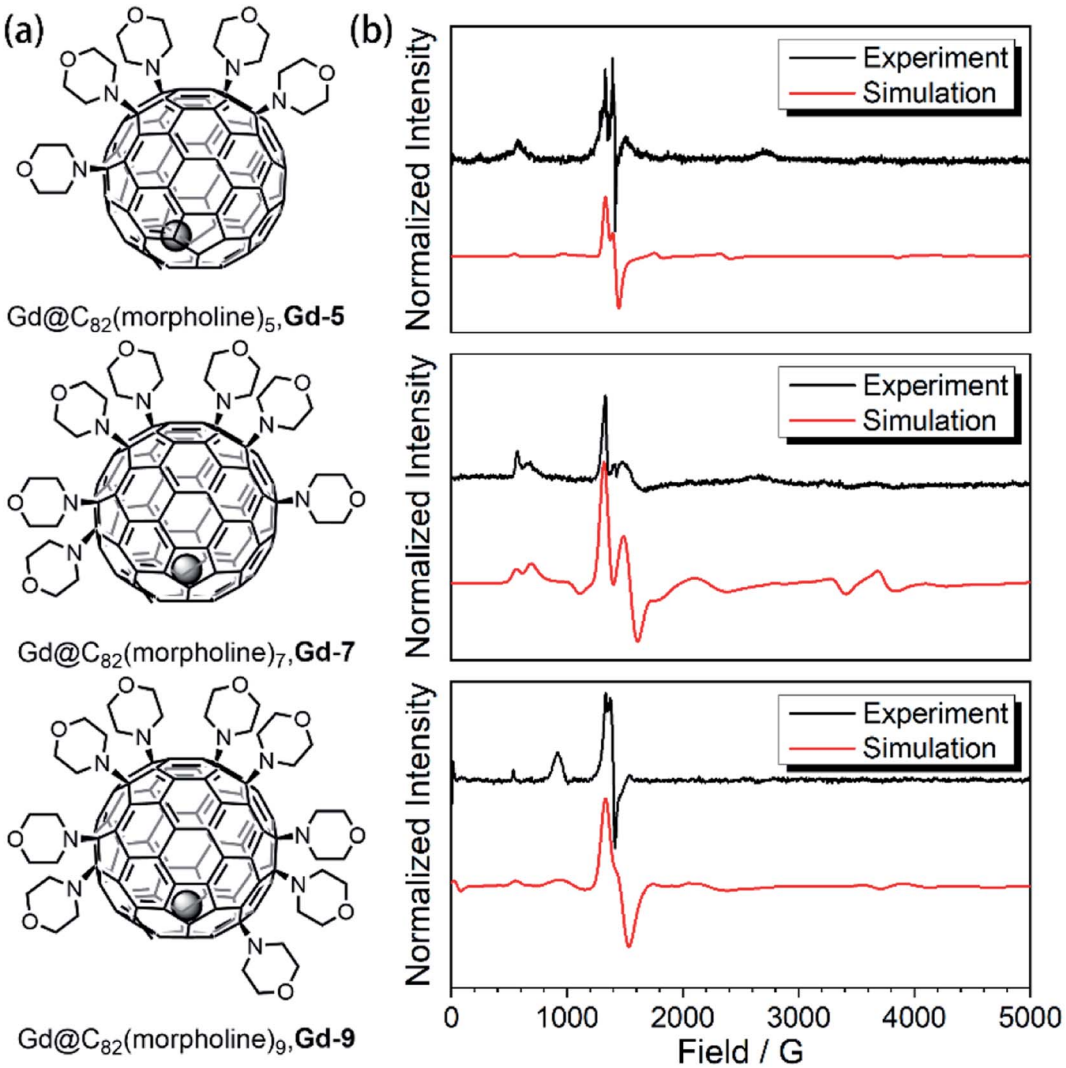

Fig. 1 (a) Aminated derivatives of Gd@C_{82} with different numbers of morpholine groups. (b) The cw-EPR measurements for the Gd-*n* derivatives (black) and the best simulation results (red).

(π/2–τ–π–τ–echo with π/2- and π-pulses of 16 and 32 ns, respectively) was used to record the electron spin echo intensities from 1 to 4000 G for **Gd-*n*** at 5 K.

As shown in Fig. 2a, several transitions at different magnetic fields can be observed. In the measurements of electron spin T_M at 5 K, one can observe that the T_M values strongly depend on the external magnetic field (B_0) as shown in Fig. 2b–e. It can be clearly seen that Gd@C_{82} shows a different pattern compared to the three derivatives. These patterns are mainly influenced by the electronic structures and the surrounding environments. Peaks in the vertical cuts indicate the resonance magnetic fields, representing the transitions which can be calculated from the spin Hamiltonian parameters. In a certain applied magnetic field, the decay of the spin echo is modulated at frequencies that depend on the field, which is attributed to the electron-spin echo envelope modulation (ESEEM) effect. The horizontal cuts of all the compounds show the modulations shown in Fig. 2f. By choosing the same B_0, the spin echoes oscillate at the same frequency, which represents the same influences from the surrounding nuclear spins. The Fourier transformations of the pattern of **Gd-5** are shown in Fig. 3b. The slope of 6.59 MHz T^{-1} indicates that the electron spin is coupled to the deuterium nuclei from the solvent ($\gamma_D = 6.5359$ MHz T^{-1}).

The temperature dependence of electron spin quantum coherence properties was investigated at the B_0 field that gave the biggest transition probabilities and therefore the strongest signals. Based on the determined spin Hamiltonian parameters, the transition assignment at various magnetic fields can be easily calculated. For Gd@C_{82}, the transition between $|-1/2\rangle$ and $|+1/2\rangle$ at 345 G was selected, and for the three derivative compounds, the transitions between $|+1/2\rangle$ and $|+3/2\rangle$ at around 1400 G were selected.

Quantum coherence behaviors

The spin echo can be observed up to 40 K for the three derivatives. T_1 and T_M at different temperatures are shown in Fig. 3. It

Open Access Article. Published on 28 mai 2020. Downloaded on 02.06.2026 07.23.18.
This article is licensed under a Creative Commons Attribution 3.0 Unported Licence.

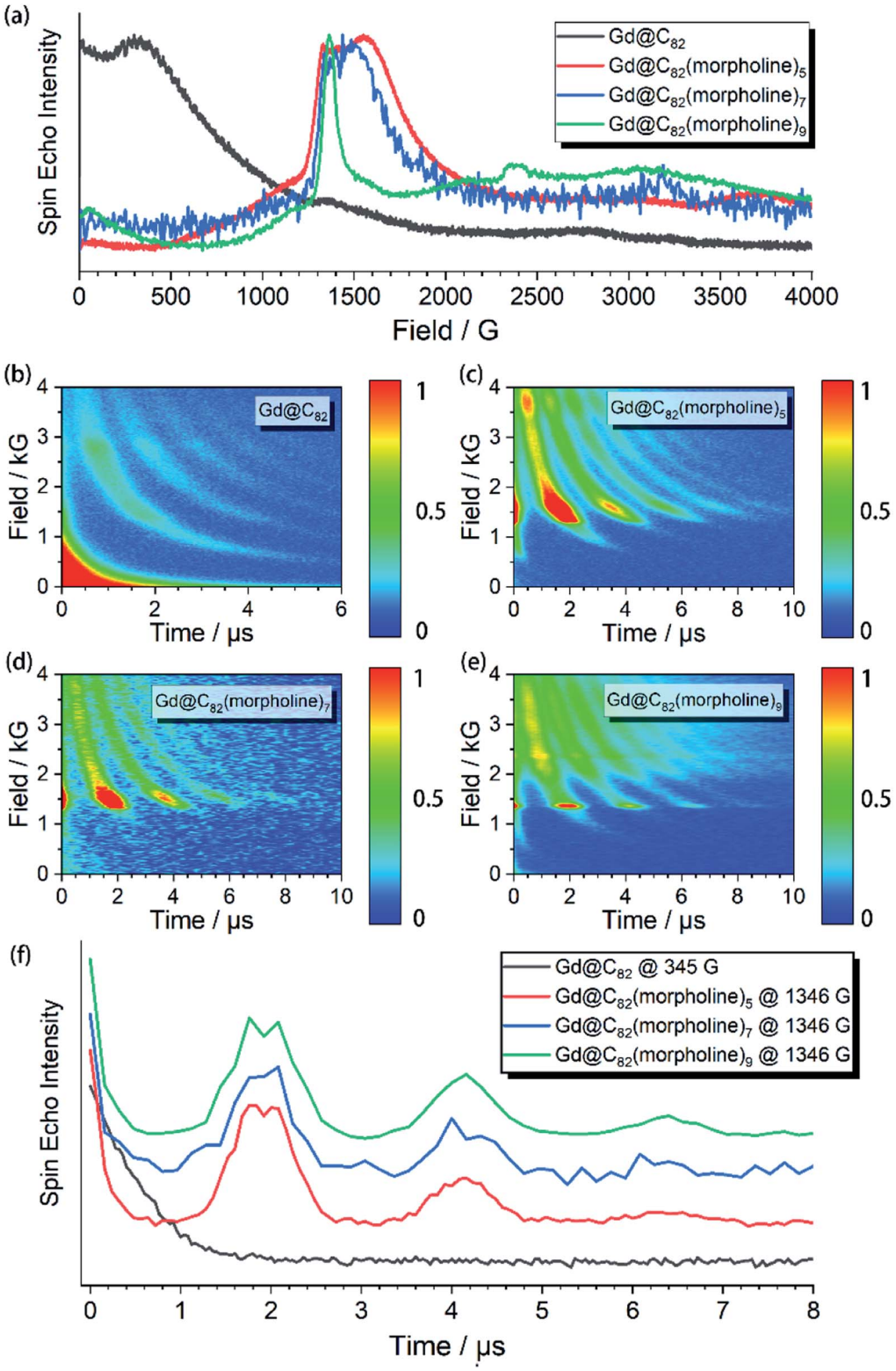

Fig. 2 (a) Echo-detected field swept spectra of Gd@C_{82} and the three derivatives **Gd-*n*** with normalized echo intensities; (b)–(e) the spin echo decay at different external applied magnetic fields (B_0) of each compound; (f) decay of the Hahn-echo intensity as a function of delay time for Gd@C_{82} and the three derivatives **Gd-*n*** at specific B_0.

can be clearly seen that both T_1 and T_M show clear response to the environment temperature. The T_1 of Gd@C_{82} is two orders of magnitude smaller than that of **Gd-*n***. The delocalized radical efficiently enhances the interaction between the electron spin and the environment. As a result, the thermally activated spin–lattice relaxation is therefore largely accelerated *via* the strong

This journal is © The Royal Society of Chemistry 2020

Open Access Article. Published on 28 mai 2020. Downloaded on 02.06.2026 07.23.18.
This article is licensed under a Creative Commons Attribution 3.0 Unported Licence.

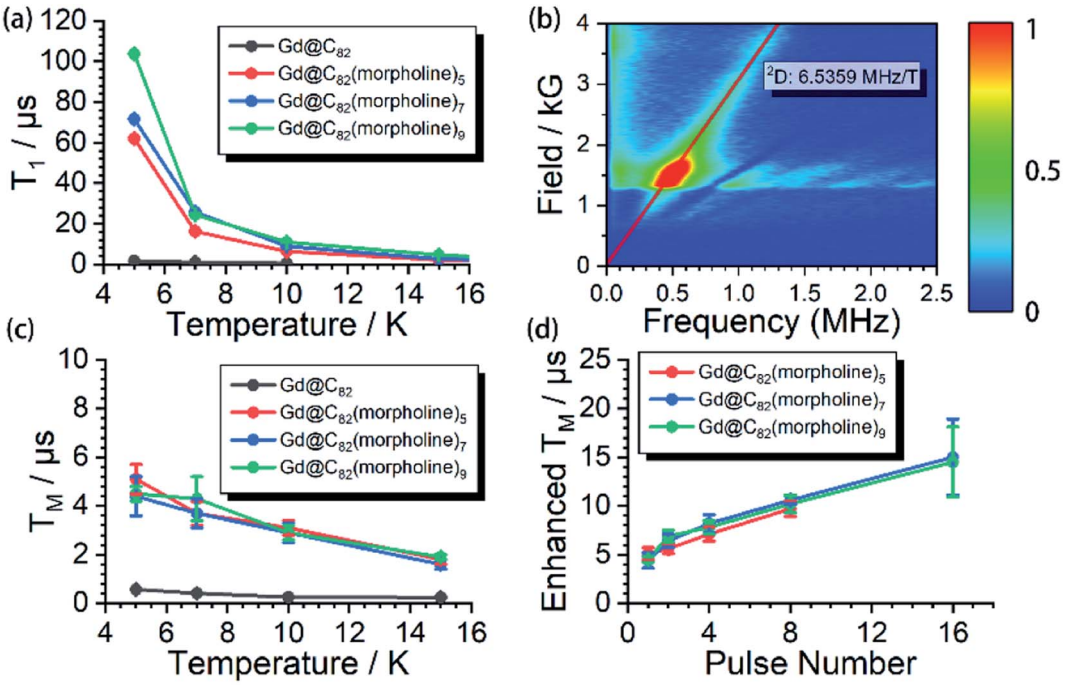

Fig. 3 (a) Spin–lattice relaxation time (T_1) of Gd@C_{82} and the three derivatives **Gd-*n***. (b) 2p-ESEEM spectrum at different external applied magnetic fields for **Gd-5**. The red line represents the simulation with the Lamour frequency of the ^{2}D nuclear spin. (c) Spin–lattice relaxation time (T_1) of Gd@C_{82} and the three derivatives **Gd-*n***. (d) Dynamic decoupling results for the three derivatives **Gd-*n***.

exchange of phonons between the cage and the environment. However in contrast, the phonon exchange between the inner magnetic ion and the environment is much less efficient, affording longer spin–lattice relaxation times in the derivatives due to the isolated spin environment. At a lower temperature of 5 K, T_1 values of all **Gd-*n*** derivatives are around 100 μs and decrease to less than 1 μs upon warming to 40 K. Within the three analogs, T_1 increases obviously with more substitution groups. This is probably due to the tougher restrictions imposed on the molecular tumbling. Fullerenes with more substitutions would have slower molecular tumbling rates,[27] which influence the rate of the vertical relaxation.[28] In our experiments, this effect of having more substitution groups appears to slow down the spin–lattice relaxation.

The quantum coherence properties of these endohedral fullerenes are also distinguishable. Due to the strong coupling with the environment arising from the radical of the outer shell, the T_M of only 1.4 μs was observed for Gd@C_{82} at 5 K and dropped below 1 μs upon warming. Nevertheless, the T_M of the high spin derivatives with quenched radicals can be enhanced to more than 5 μs, which are even better than those of VO^{2+} ($S = 1/2$) and Cr^{3+} ($S = 3/2$) based low spin molecules.[29–31] The temperature dependence of the quantum phase memory time shows a different trend compared to the spin–lattice relaxation time. Upon warming from 5 K to 10 K, T_M decreases slightly for the three analogs. Different from the strong relation between T_1 and temperature, the decoherence of the electron spin superposition state is caused by additional sources, including the dipolar interaction between the investigated electron spin and the environmental nuclear or electron spins.[32,33] The molecular concentrations in these experiments were low enough to consider that the electron spin dipolar–dipolar interaction was a minor effect that resulted in the decoherence path here.[34] The aforementioned ESEEM effects indicate that the electron spin of Gd^{3+} is effectively coupled to the environment nuclei. Based on these analyses, we confirm that the hyperfine coupling of the nuclear spins dominates the decoherence of the electron spin superposition states in the three derivatives at relatively low temperatures from 5 to 10 K. By warming up the spin system above 10 K, T_M decreases with the same trend as T_1. The T_1 of each molecule is around twice of T_M, and even closer at higher temperatures. Therefore, the thermal process becomes the main decoherence path above 10 K. It is also interesting to compare the quantum coherence time of the three derivatives. The molecule with the least number of substituted morpholine groups shows the longest phase memory time at 5 K. While upon warming, the T_M of **Gd-5** drops more rapidly than that of the other two. This is mainly due to the T_1 limitation, indicating that the molecules with a longer spin–lattice relaxation time are less limited at relatively higher temperatures.

Dynamic decoupling

The nuclear spins around the electron spin can generate the local Overhauser field which oscillates at Larmor frequencies. As discussed previously, these nuclear spins acted as the major decoherence path in our experiment at relatively low temperatures. This unwanted environment effect can be decoupled by employing a train of refocusing pulses before the detection of the spin echo.[35] Here, the CPMG-*n* pulse sequence was applied

Open Access Article. Published on 28 mai 2020. Downloaded on 02.06.2026 07.23.18.
This article is licensed under a Creative Commons Attribution 3.0 Unported Licence.

to the three derivatives at 5 K, where n represents the number of the inversion pulses. This dynamic decoupling pulse sequence exhibits very efficient enhancement of T_M. By applying up to 16 inversion pulses, the phase memory times were successfully extended to nearly 20 μs, which is 4 fold higher compared to the original phase memory times. These dynamic decoupling experiments suggest that by employing refocusing pulses, the interactions between electrons and surrounding nuclear spins are successfully decoupled. It is also worth noting that T_M can be further extended with more than 16 refocusing pulses; however, the detection is limited by the weak signals.

Conclusions

In summary, the quantum coherence behaviors of the three derivative compounds of the endohedral fullerene Gd@C_{82} with an odd number of morpholine groups, Gd@C_{82}(morpholine)$_n$ (n = 5, 7 and 9), have been investigated using pulse-EPR. By quenching the radical located at the carbon cage, the electronic structures become largely different from those of the original Gd@C_{82}. The quantum phase memory times (T_M) can be enhanced to more than 5 μs at 5 K which are even better compared to that of low spin molecules. While, with the increasing number of substitution groups, spin–lattice relaxation times (T_1) also show significant enhancement due to the interaction variation between the molecules and environment. Besides, it is also worth noting that T_M show no obvious difference below 10 K, while they are limited by T_1 at higher temperatures. Gd^{3+} based endohedral fullerenes have been widely used in interesting studies including medical development and quantum information processing, and precisely controlling the quantum coherence properties are required for better applications. In this work, **Gd-*n*** derivative compounds can act as an appropriate model to investigate the quantum coherence behaviors with tunable environmental influences. We successfully find the relationship between the molecule structures and quantum coherence behaviors and give suggestions on designing particular molecules for certain applications. By taking advantage of paramagnetic endohedral fullerenes, we believe such chemical engineering can enrich the interests in molecular design.

Experimental

Synthesis and isolation

The samples were synthesized and purified as described in our previous work.[23,24]

EPR measurements

Gd@C_{82} and the three derivatives were dissolved in d_8-toluene for EPR experiments with a spin concentration of 0.012 mmol L^{-1} determined by the spin counting method. The cw-EPR spectra were measured on a Bruker Elexsys E580 spectrometer with a superhigh sensitivity probehead (ω = 9.36 GHz). Pulsed EPR data were collected on the same system using an MS-3 cavity (ω = 9.33 GHz). The low-temperature environment was achieved using Oxford Instruments liquid helium cryostats (ESR900 for cw and CF935 for pulse). The cw-EPR spectra were simulated using an EasySpin[36] toolbox (http://www.easyspin.org/) based on MATLAB. The signals of the pulsed-EPR experiments were collected by integrating the Hahn echo ($\pi/2$–τ–π–τ–echo) with τ = 200 ns. The T_1 values were measured by the inversion recovery method (π–T–$\pi/2$–τ–π–τ–echo) with 4-step phase cycling. The T_M values were obtained by increasing the τ value of the Hahn echo sequence with 4-step phase cycling. The ESEEM measurements were carried out using the 2p ESEEM sequence ($\pi/2$–τ–π–τ–echo) with 4-step phase cycling. The dynamic decoupling measurements were carried out using the CPMG-n sequence ($\pi/2_x$–(τ–π_y–τ)$_n$–echo) with 4-step phase cycling. The $\pi/2$ and π pulse lengths in EDFS, T_1 and T_M measurements were 16 and 32 ns with 9 dB attenuation of the microwave power of 300 W, respectively.

Magnetic measurements

The powder samples of **Gd-7** with exact mass for DC magnetic measurements were wrapped in parafilm and fixed in a capsule. DC experiments were performed on a Quantum Design MPMS XL-5 SQUID magnetometer. Magnetic data were corrected for the paramagnetism from the parafilm and capsule, and the diamagnetic contribution of the sample was calculated from Pascal's constants. The magnetization and magnetic susceptibility data were simulated using an EasySpin toolbox[36] (http://www.easyspin.org/) based on MATLAB.

Author contributions

Z. L. performed the EPR and magnetic measurements, assisted by B.-W. D. H. H. and B.-Y. S. prepared and purified the sample for measurements. Z. L. processed and analyzed the EPR and magnetic data. The project was conceived by S. G. and S.-D. J. Z. L. and S.-D. J. designed the experiments and wrote the manuscript. All the authors revised the manuscript.

Conflicts of interest

The authors declare no conflict of interest.

Acknowledgements

This research was supported by the National Natural Science Foundation of China (21822301, 21971242, and 11705211), National Basic Research Program of China (2018YFA0306003, 2017YFA0204903, 2016YFA0203200 and 2018YFA0703504), Beijing Academy of Quantum Information Sciences (Y18G23) and Young Scientist Innovative Foundation of IHEP (E05469U2, and Y95461C).

References

1 P. Jin, Y. Li, S. Magagula and Z. Chen, *Coord. Chem. Rev.*, 2019, **388**, 406–439.
2 T. Wang and C. Wang, *Small*, 2019, **15**, 1901522.

 This journal is © The Royal Society of Chemistry 2020

Open Access Article. Published on 28 mai 2020. Downloaded on 02.06.2026 07.23.18.
This article is licensed under a Creative Commons Attribution 3.0 Unported Licence.

3 W. Cai, C.-H. Chen, N. Chen and L. Echegoyen, *Acc. Chem. Res.*, 2019, **52**, 1824–1833.
4 G. Liu, S.-H. Liou, N. Enkin, I. Tkach and M. Bennati, *Phys. Chem. Chem. Phys.*, 2017, **19**, 31823–31829.
5 K. B. Ghiassi, M. M. Olmstead and A. L. Balch, *Dalton Trans.*, 2014, **43**, 7346–7358.
6 H. Kato, K. Suenaga, M. Mikawa, M. Okumura, N. Miwa, A. Yashiro, H. Fujimura, A. Mizuno, Y. Nishida, K. Kobayashi and H. Shinohara, *Chem. Phys. Lett.*, 2000, **324**, 255–259.
7 L. Spree and A. A. Popov, *Dalton Trans.*, 2019, **48**, 2861–2871.
8 I. Rašović, *Mater. Sci. Technol.*, 2017, **33**, 777–794.
9 W. Zhang, B. Sun, L. Zhang, B. Zhao, G. Nie and Y. Zhao, *Nanoscale*, 2011, **3**, 2636.
10 P. W. Shor, in *Proceedings 35th Annual Symposium on Foundations of Computer Science*, IEEE Comput. Soc. Press, Santa Fe, NM, USA, 1994, pp. 124–134.
11 L. M. K. Vandersypen, M. Steffen, G. Breyta, C. S. Yannoni, M. H. Sherwood and I. L. Chuang, *Nature*, 2001, **414**, 883–887.
12 V. L. Ermakov and B. M. Fung, *Phys. Rev. A: At., Mol., Opt. Phys.*, 2002, **66**, 042310.
13 A. Gaita-Ariño, F. Luis, S. Hill and E. Coronado, *Nat. Chem.*, 2019, **11**, 301–309.
14 M. N. Leuenberger and D. Loss, *Nature*, 2001, **410**, 789–793.
15 G. Aromí, D. Aguilà, P. Gamez, F. Luis and O. Roubeau, *Chem. Soc. Rev.*, 2012, **41**, 537–546.
16 J. J. L. Morton, A. M. Tyryshkin, A. Ardavan, K. Porfyrakis, S. A. Lyon and G. A. D. Briggs, *J. Chem. Phys.*, 2006, **124**, 014508.
17 R. M. Brown, Y. Ito, J. H. Warner, A. Ardavan, H. Shinohara, G. A. D. Briggs and J. J. L. Morton, *Phys. Rev. B: Condens. Matter Mater. Phys.*, 2010, **82**, 033410.
18 Z. Liu, B.-W. Dong, H.-B. Meng, M.-X. Xu, T.-S. Wang, B.-W. Wang, C.-R. Wang, S.-D. Jiang and S. Gao, *Chem. Sci.*, 2018, **9**, 457–462.
19 Z. Hu, B.-W. Dong, Z. Liu, J.-J. Liu, J. Su, C. Yu, J. Xiong, D.-E. Shi, Y. Wang, B.-W. Wang, A. Ardavan, Z. Shi, S.-D. Jiang and S. Gao, *J. Am. Chem. Soc.*, 2018, **140**, 1123–1130.
20 S. Zhou, I. Rašović, G. A. D. Briggs and K. Porfyrakis, *Chem. Commun.*, 2015, **51**, 7096–7099.
21 S. Zhou, M. Yamamoto, G. A. D. Briggs, H. Imahori and K. Porfyrakis, *J. Am. Chem. Soc.*, 2016, **138**, 1313–1319.
22 K. Furukawa, S. Okubo, H. Kato, H. Shinohara and T. Kato, *J. Phys. Chem. A*, 2003, **107**, 10933–10937.
23 H. Huang, L. Zhang, X. J. Gao, X. Guo, R. Cui, B. Xu, J. Dong, Y. Li, L. Gan, F. Chang, X. Gao and B. Sun, *Chem. Mater.*, 2018, **30**, 64–68.
24 H. Huang, Z. Liu, L. Zhang, X. Guo, R. Cui, J. Dong, F. Chang, S. Jiang, S. Gao and B. Sun, *Carbon*, 2020, **158**, 320–326.
25 M. D. Jenkins, Y. Duan, B. Diosdado, J. J. García-Ripoll, A. Gaita-Ariño, C. Giménez-Saiz, P. J. Alonso, E. Coronado and F. Luis, *Phys. Rev. B*, 2017, **95**, 064423.
26 E. Moreno-Pineda, C. Godfrin, F. Balestro, W. Wernsdorfer and M. Ruben, *Chem. Soc. Rev.*, 2018, **47**, 501–513.
27 G. Liu, M. d. C. Gimenez-Lopez, M. Jevric, A. N. Khlobystov, G. A. D. Briggs and K. Porfyrakis, *J. Phys. Chem. B*, 2013, **117**, 5925–5931.
28 *The essential physics of medical imaging*, ed. J. T. Bushberg, Wolters Kluwer Health/Lippincott Williams & Wilkins, Philadelphia, 3rd edn, 2012.
29 M. J. Graham, J. M. Zadrozny, M. Shiddiq, J. S. Anderson, M. S. Fataftah, S. Hill and D. E. Freedman, *J. Am. Chem. Soc.*, 2014, **136**, 7623–7626.
30 J. M. Zadrozny, J. Niklas, O. G. Poluektov and D. E. Freedman, *J. Am. Chem. Soc.*, 2014, **136**, 15841–15844.
31 M. S. Fataftah, J. M. Zadrozny, S. C. Coste, M. J. Graham, D. M. Rogers and D. E. Freedman, *J. Am. Chem. Soc.*, 2016, **138**, 1344–1348.
32 W. Wernsdorfer, *Nat. Mater.*, 2007, **6**, 174–176.
33 A. Morello, P. C. E. Stamp and I. S. Tupitsyn, *Phys. Rev. Lett.*, 2006, **97**, 207206.
34 A. Ardavan, O. Rival, J. J. L. Morton, S. J. Blundell, A. M. Tyryshkin, G. A. Timco and R. E. P. Winpenny, *Phys. Rev. Lett.*, 2007, **98**, 057201.
35 S. Meiboom and D. Gill, *Rev. Sci. Instrum.*, 1958, **29**, 688–691.
36 S. Stoll and A. Schweiger, *J. Magn. Reson.*, 2006, **178**, 42–55.